Switchable electro-optic diffractive lens with high efficiency for ophthalmic applications

Guoqiang Li*†, David L. Mathine*, Pouria Valley*, Pekka Äyräs*, Joshua N. Haddock‡, M. S. Giridhar*, Gregory Williby*, Jim Schwiegerling*§, Gerald R. Meredith*, Bernard Kippelen‡, Seppo Honkanen*, and Nasser Peyghambarian*†

*College of Optical Sciences, University of Arizona, Tucson, AZ 85721; ‡School of Electrical and Computer Engineering, Georgia Institute of Technology, Atlanta, GA 30332; and §Department of Ophthalmology and Vision Sciences, University of Arizona, Tucson, AZ 85711

Communicated by Nicolaas Bloembergen, University of Arizona, Tucson, AZ, February 2, 2006 (received for review December 10, 2005)

Presbyopia is an age-related loss of accommodation of the human eye that manifests itself as inability to shift focus from distant to near objects. Assuming no refractive error, presbyopes have clear vision of distant objects; they require reading glasses for viewing near objects. Area-divided bifocal lenses are one example of a treatment for this problem. However, the field of view is limited in such eyeglasses, requiring the user to gaze down to accomplish near-vision tasks and in some cases causing dizziness and discomfort. Here, we report on previously undescribed switchable, flat, liquid-crystal diffractive lenses that can adaptively change their focusing power. The operation of these spectacle lenses is based on electrical control of the refractive index of a 5-μm-thick layer of nematic liquid crystal using a circular array of photolithographically defined transparent electrodes. It operates with high transmission, low voltage (<2 V_{rms}), fast response (<1 sec), diffraction efficiency > 90%, small aberrations, and a power-failure-safe configuration. These results represent significant advance in state-of-the-art liquid-crystal diffractive lenses for vision care and other applications. They have the potential of revolutionizing the field of presbyopia correction when combined with automatic adjustable focusing power.

ophthalmic lens | switchable lens | vision correction

The use of nematic liquid crystals to implement switchable lenses has been proposed previously but had limited success for ophthalmic applications (1). Hybrid liquid-crystal refractive lenses incorporating convex and concave substrates have been demonstrated (2, 3). However, the large thickness of the liquid-crystal layers (>400 μm) make their response and recovery times long and their transmission low because of optical scattering. To reduce the thickness of the active layer, surface relief Fresnel lens substrates have been proposed (4). However, in this geometry the lens is optically active in the electrically off-state, which is not desirable for ophthalmic applications where a loss of electrical power could suddenly result in near-vision correction during a critical distance vision task such as driving. In other approaches, thin uniform layers of liquid crystal were used, and refractive lenses were produced by the use of discrete electrodes (5), continuous highly resistive electrodes (6), or spatially distributed electric fields (microlenses) (7). However, in these lenses either the range of focal length or their small diameter made them unsuitable for ophthalmic applications. We employ a photolithographically patterned thin diffractive lens with large aperture, fast response time, and a power-failure-safe configuration to overcome these limitations. Although high-efficiency liquid-crystal-based diffractive devices have been demonstrated for beam-steering (8, 9), less effort was given to the development of switchable diffractive lenses. The diffraction efficiencies of the lenses achieved for imaging (10–15) and other applications (16, 17) were too low to meet the requirements of ophthalmic applications.

Fig. 1*a* compares the shape (phase profile) of a refractive lens (dashed line) with an ideal diffractive lens (dotted line). The diffractive lens is produced by removing the multiple 2π-phase retardation from the refractive lens, resulting in multiple Fresnel zones. The phase jump at each zone boundary is 2π for the design wavelength. The outer radius of each zone is given by (18)

$$r_m = \sqrt{2m\lambda f}, \quad m = 1, 2, \ldots, M, \qquad \textbf{[1a]}$$

where m is a counting index that refers to successive Fresnel zone starting in the center, λ is the wavelength, and f is the focal length. To digitize the process, the continuous phase profile in each zone is divided into multiple subzones with a series of discrete phase levels (19) ("staircase" structure; Fig. 1*a*). The outer radius of each subzone is given by

$$r_{m,n} = \sqrt{2[(m-1) + n/L]\lambda f}, \quad n = 1, 2, \ldots, L, \qquad \textbf{[1b]}$$

where L is the number of phase levels per zone, and n is the counting index of the individual phase levels. Diffraction efficiency increases by increasing the number of subzones L, reaching maximum values of 40.5%, 81.1%, and 95.0% for lenses with two, four, and eight phase levels per zone, respectively.

Diffractive lenses with eight subzones, 10-mm diameters, and focal lengths of 1 and 0.5 m (+1.0 and +2 diopter of add power, respectively) were demonstrated at the peak of the human photopic response, 555 nm. The schematic drawings of the electrode pattern and the fabrication procedure are shown in Fig. 1 *b* and *c*, respectively. Using photolithographic techniques, concentric and rotationally symmetric transparent indium tin oxide electrodes (50 nm in thickness), whose radii were determined by Eq. **2**, were patterned on a float-glass substrate. A 1-μm gap was required between adjacent electrodes to maintain electrical isolation and ensure a smooth transition of the phase profile introduced by the liquid crystal. Over the patterned indium tin oxide, a 200-nm-thick electrically insulating layer of SiO_2 is sputtered and into which small via openings (3×3 μm) were etched, allowing electrical contact to be made to the underlying electrodes. An electrically conductive layer of Al is subsequently sputtered over the insulating layer to fill the vias and contact the electrodes and patterned to form eight independent electrical bus bars (6-μm wide within the lens). Each bus bar connects the discrete phase level electrodes of equal counting index n in all Fresnel zones (as shown in Fig. 1*b*) such that only eight external electrical connections (plus one ground connection) are required per lens.

The patterned substrate, as well as an additional substrate with a continuous indium tin oxide electrode that acts as the electrical ground, were spin coated with poly(vinyl alcohol) to act as liquid-crystal alignment layer. The alignment layers were rubbed with a velvet cloth to achieve homogeneous alignment, and the two substrates were assembled. The commercial nematic liquid

Conflict of interest statement: No conflicts declared.

Abbreviation: MTF, modulation transfer function.

†To whom correspondence may be addressed. E-mail: gli@optics.arizona.edu or nnp@optics.arizona.edu.

www.pnas.org/cgi/doi/10.1073/pnas.0600850103

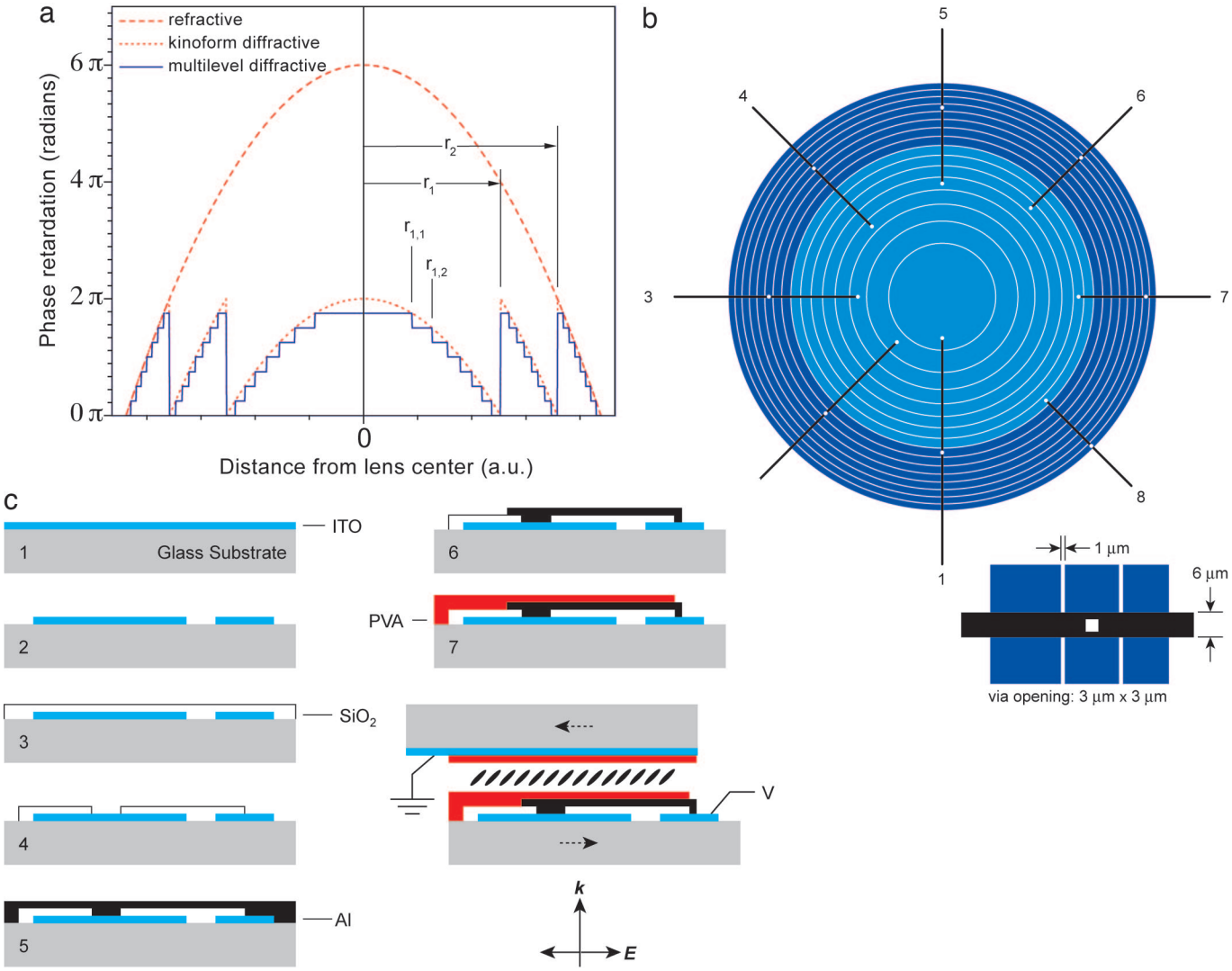

Fig. 1. Adaptive liquid-crystal diffractive lens. (*a*) Dashed line, phase profile of a conventional refractive lens; dotted line, phase profile to achieve a diffractive lens; staircase structure, multilevel quantization approximates the continuous quadratic blaze profile. a.u., arbitrary units. (*b*) Layout of the one-layer electrode pattern (two central zones shown). Adjacent zones are distinguished by color. An electrical insulation layer with vias is added (vias shown with white dots). Each bus connects to one electrode (subzone) in each zone. Dimensions of the vias, the bus line, and the gap between electrodes are illustrated in the lower right. (*c*) Processing steps for fabrication of the patterned electrodes and the conductive lines. The structure of the liquid-crystal lens is shown in the lower right, where *k* is the wave vector, and *E* is the polarization state of the incident light.

crystal E7 (Merck) was used as the electro-optic medium and was filled by capillary action into the empty cell at a temperature above the clearing point (60°C) and then cooled at 1°C/min to room temperature. The cell then was sealed with epoxy and connected to the drive electronics. The drive electronics consist of custom-fabricated integrated circuits that contain eight independently controlled output channels. Each channel generates a modified square waveform with variable peak-to-peak amplitude between 0 and 5 V.

Results

The lens showed excellent performance (because of space limitations, we only describe the results for the 1-diopter lens). In the optically inactive state (voltage off) in which the lens has no focusing power, optical transmission is 85% over the visible spectrum, a value that can be increased by the use of ophthalmic quality substrates and antireflection coatings. Monochromatic (543.5 nm) polarized microscopy images of the lens under operation (see *Methods*) indicate that all eight electrode sets operated properly and provided discrete phase changes (Fig. 2*a*). Eight optimized drive voltages with amplitudes between 0 and 2 V_{rms} produced a maximum first-order diffraction efficiency of 91%, near the 95% predicted by scalar diffraction theory. The measured diffraction efficiency as a function of lens area (see *Methods*) reaches 94% near the center of the lens, decreasing monotonically as the area is increased (Fig. 2*b*). The decrease is due to the fact that phase distortion caused by the fringing field at the zone boundaries has more significant effect at the outer zones as the width of each electrode becomes smaller. At the edges of the electrodes, the electric field lines are not perpendicular to the liquid-crystal lens substrate, and the fringing fields cause the phase transitions at the zone boundaries to be not as sharp as in the ideal case, thus inducing phase distortions and reducing the diffraction efficiencies (20, 21). The focused spot size is ≈135 μm, which is also close to the diffraction-limit value of 133 μm. The lens shows subsecond switching time.

Interferometric measurements at 543.5 nm (see *Methods*) show excellent imaging capability of the lens. Strong modulation

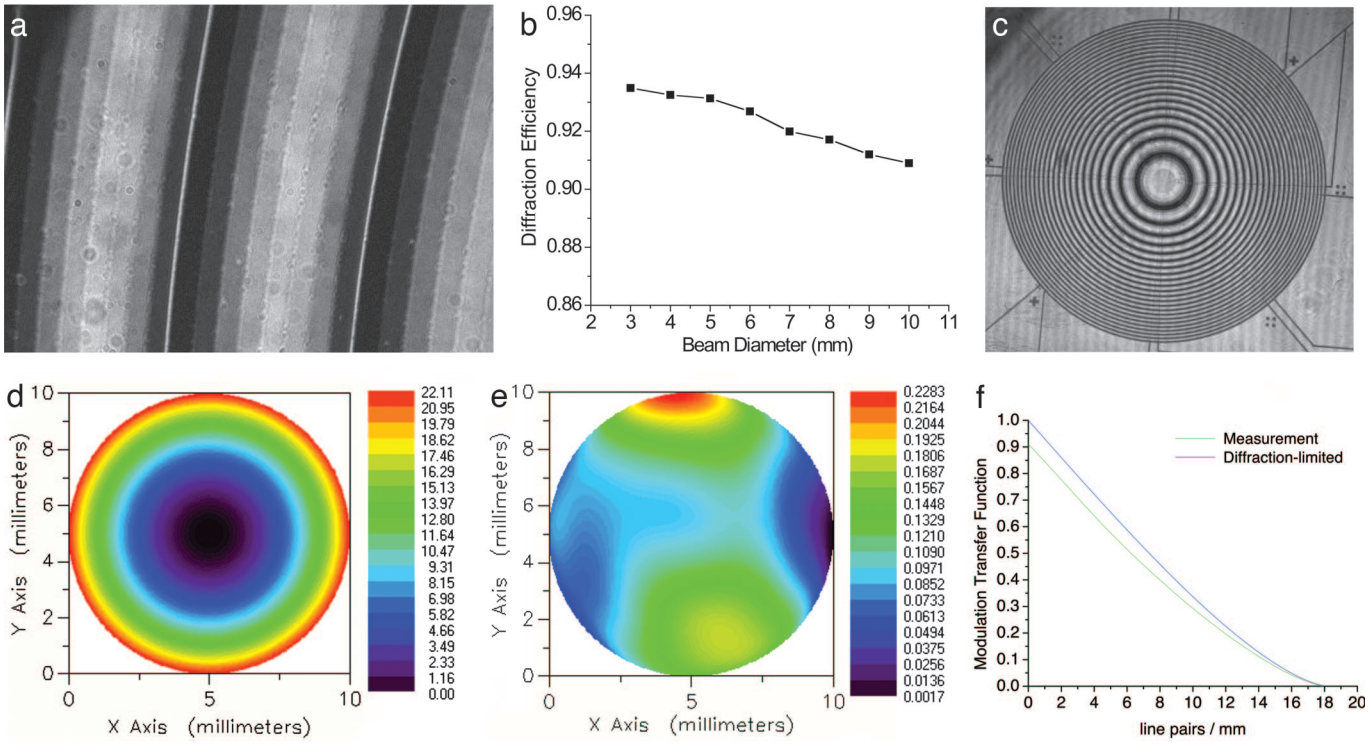

Fig. 2. Characterization of the 1-diopter lens. (*a*) Electro-optic response of the lens obtained with polarized microscope. (*b*) Diffraction efficiency as a function of the beam diameter. (*c*) Interferogram obtained with the Mach–Zehnder interferometer. The interference pattern has very good fringe modulation across the lens. A close-up view of the interferogram shows that the eight subzones in each zone have different grayscale intensities, and the pattern is periodic. (*d*) Unwrapped phase map for a 10-mm aperture. (*e*) Phase map of the unwrapped phase minus tilting and focusing. (*f*) MTF of the lens. The green line is obtained from the measurement data, and the blue line is for a diffraction-limited lens. The value at low spatial frequency is determined by the diffraction efficiency of the lens.

of the optical power is observed in interferogram of the lens in the optically active state (Fig. 2*c*). The unwrapped phase map of the lens is shown in Fig. 2*d* with a peak-to-valley optical path length of 23.05λ. The focusing power was estimated to be 1.002 diopter, in excellent agreement with the design value. Very good spherical profiles were obtained in both x and y cross sections, indicating small aberrations. Higher-order aberrations were estimated by analyzing the difference between the measured wavefront and a best-fit spherical wave and tilt (Fig. 2*e*). The peak-to-valley range of the difference is 0.241λ, and the rms value is 0.039λ, which is comparable with a high-quality reading glass. The modulation transfer function (MTF) indicated near diffraction-limited performance (Fig. 2*f*). All properties of the lens, as shown in Fig. 2, make the switchable lens suitable for ophthalmic applications.

To test the imaging properties of the lens, a model human eye was constructed by using a fixed, +60 diopter achromatic doublet glass lens and a monochrome charge-coupled device (CCD) with a filter to match the human photopic response. Because homogeneously aligned nematic liquid crystals are polarization sensitive, two lenses with orthogonal alignment directions were used in series to create a single polarization-insensitive lens. Two such lenses were aligned and cemented together. To simulate a typical near-vision task such as reading, a double-element lens was placed in front of the model eye and used to image a test object illuminated with unpolarized white light placed 30 cm in front of the lens. As can be seen in Fig. 3*a*, the model eye has insufficient power to form a sharp image, but by switching on the diffractive lens the image is brought into focus (Fig. 3*b*). The double-element lens has excellent optical transmission. To test the imaging performance of the lenses with actual human subjects, a pair of test spectacles has been constructed (Fig. 4), and initial clinical results agree well with the model eye test. When the electro-optic lenses are both in the inactive state, there is no noticeable degradation in the quality of the distant vision. For chromatic aberration, an achromatic diffractive lens can be designed by introducing $p2\pi$ ($p > 1$, integer) phase jump at the zone boundaries for the design wavelength (22). In practice, the ocular lens itself has a chromatic aberration that is less than the diffractive lens. Assuming the brain is adapted to a certain degree of chromatic aberration, balancing the dispersion of the diffractive lens and the eye is less desirable. More clinical study needs to be performed on this aspect.

Conclusion

In conclusion, we have demonstrated switchable liquid-crystal diffractive lenses with high diffraction efficiency, high optical quality, rapid response time, and diffraction-limited performance. These flat lenses are highly promising to replace conventional area division refractive, multifocal spectacle lenses used by presbyopes. They have the potential of revolutionizing the field of presbyopia correction when it is combined with automatic adjustable focusing power. Negative focusing powers also can be achieved with the same lenses by changing the sign of the slope of the applied voltages. The use of these lenses is not limited to ophthalmology but can be extended to numerous other applications including dentistry where switchable lens elements with relatively large diameters are desirable.

Methods

When the device is fabricated, various optical characterizations are performed.

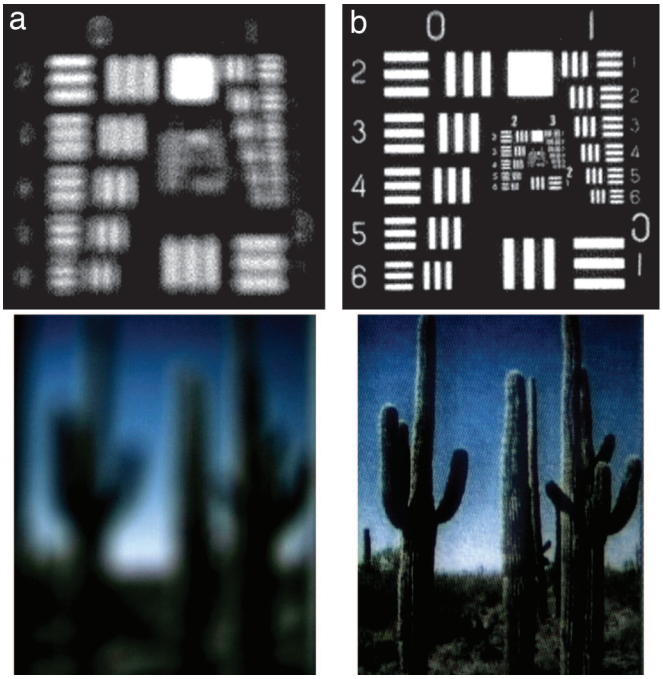

Fig. 3. Hybrid imaging using the 1-diopter electroactive diffractive lens with the model eye. The function of the diffractive lens is to provide near-vision correction to the model eye. (*a*) The object is placed at a reading distance (≈30 cm). The image is severely out of focus in the model eye when the diffractive lens is off. (*b*) When the diffractive lens is activated, the object is imaged clearly.

Polarized Microscopy. A computer-interfaced polarized optical microscope with a laser source at 543.5 nm was constructed on the optical bench and used to inspect the lenses on a microscopic scale and verify that all electrodes were operating properly. The lens was placed between crossed polarizers where the transmission axes were oriented at angles of 45° and −45° with respect to the liquid-crystal alignment layer rub direction. For each position on the lens, the intensity seen by the charge-coupled device camera is a function of the voltage-dependent phase retardation $\phi(V)$ between the ordinary and extraordinary wave components at the exit surface of the lens. The voltage dependent transmission between crossed polarizers $[T(V)]$ is given by

$$T(V) = \sin^2\left(\frac{\phi(V)}{2}\right), \qquad [2]$$

where the transmission is a maximum when $\phi(V) = \pi$ and a minimum when $\phi(V) = 2\pi$ (23). Therefore, the voltage-dependent phase retardation of each electrode can be inspected by observing the intensity variations over its area.

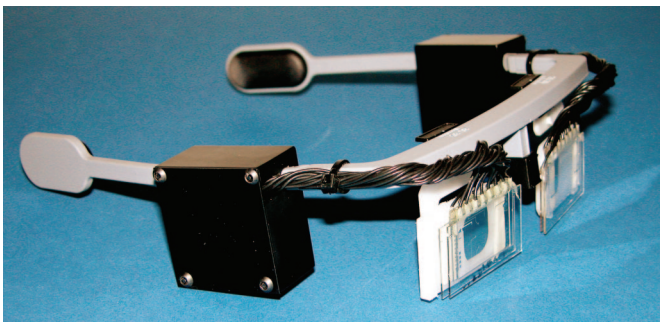

Fig. 4. A prototype of the assembled adaptive eyewear.

Measurement of Diffraction Efficiency. Diffraction efficiency is the amount of light intensity that goes to a particular diffraction order compared with the sum of intensities in all of the diffraction orders. To determine the efficiency of the first diffracted order, a linearly polarized 543.5-nm laser beam was expanded to a diameter of 10 mm and allowed to pass through the active area of the lens. The power of the beam was measured in the focal plane with the lens inactive (total power) and then again with the lens activated (diffracted power). The ratio of diffracted power to total power is the diffraction efficiency. A small aperture in front of the detector was used to isolate the first-order light when the lens was activated, and as all measurements were made down-stream of the lens, they were automatically corrected for Fresnel losses. To measure the diffraction efficiency as a function of lens area, a variable aperture (positioned concentrically with respect to the lens) was placed in front of the diffractive lens to control the size of the beam. The diffraction efficiency then was measured as the diameter of the beam was increased from 3 to 10 mm in 1-mm increments.

Interferometric Testing and MTF Calculation. The performance of the diffractive lenses also was evaluated by using a computer-interfaced, phase-shifting Mach–Zehnder interferometer with a linearly polarized 543.5-nm laser source (24, 25). The lens under test was placed in the object arm of the interferometer and then imaged onto a charge-coupled device camera such that the captured interference patterns were formed by the converging wavefront generated at the exit face of the lens and the reference plane wave. A small aperture was placed between the imaging lens and the camera at the point of focus to isolate and test only the wavefront generated by the first diffracted order. Multiple $\pi/2$ phase shifts were generated in the reference arm by using a piezoelectric transducer actuated mirror, and a phase unwrapping algorithm then was used to generate a phase map of the diffracted wavefront. From this unwrapped phase map of the wavefront immediately behind the diffractive lens, the focal length (f) of the diffractive lens is calculated by using

$$f = \frac{\rho^2}{2OPD}, \qquad [3]$$

where OPD is the peak-to-valley optical path difference from center to edge, and ρ is the radius of the test area (26). Because the lenses were designed for operation at 555 nm but tested at 543.5 nm, correction of the extracted focal length value was made by

$$f(\lambda) = f_0\frac{\lambda_0}{\lambda}, \qquad [4]$$

where f_0 and λ_0 are the design focal length and wavelength, respectively, and λ is the measurement wavelength (27). Measurement of the peak-to-valley and rms errors in the wavefront were made subsequent to removing the best-fit sphere and any tilt from the phase map.

The imaging performance of the lens can be evaluated in terms of MTF, which represents the ratio of the image modulation to the object modulation at all frequencies. The wavefront of the first-order diffraction can be expressed by a sum of Zernike polynomials (28), and the MTF thus can be calculated by normalized autocorrelation of the generalized pupil function (26).

We thank the Technology and Research Inititative Fund program of the State of Arizona.

1. Smith, G. & Atchison, D. A. (1997) *The Eye and Visual Optical Instruments* (Cambridge Univ. Press, Cambridge, U.K.).
2. Sato, S. (1985) *Jpn. J. Appl. Phys.* **18,** 1679–1684.
3. Fowler, C. W. & Pateras, E. S. (1990) *Ophthal. Physiol. Opt.* **10,** 186–194.
4. Sato, S., Sugiyama, A. & Sato, R. (1985) *Jpn. J. Appl. Phys.* **24,** L626–L628.
5. Kowel, S. T., Cleverly, D. S. & Kornreich, P. G. (1984) *Appl. Opt.* **23,** 278–289.
6. Naumov, A. F., Loktev, M. Y., Guralnik, I. R. & Vdovin G. (1998) *Opt. Lett.* **23,** 992–994.
7. Masuda, S., Takahashi, S., Nose, T., Sato, S. & Ito H. (1997) *Appl. Opt.* **36,** 4772–4778.
8. Friedman, L. J., Hobbs, D. S., Lieberman, S., Corkum, D. L., Nguyen, H. Q., Resler, D. P., Sharp, R. C. & Dorschner, T. A. (1996) *Appl. Opt.* **35,** 6236–6240.
9. Resler, D. P., Hobbs, D. S., Sharp, R. C., Friedman, L. J. & Dorschner, T. A. (1996) *Opt. Lett.* **21,** 689–691.
10. Williams, G., Powell, N. J. & Purvis, A. (1989) *Proc. SPIE* **1168,** 352–357.
11. Patel, J. S. & Rastani, K. (1991) *Opt. Lett.* **16,** 532–534.
12. Dance, B. (1992) *Laser Focus World* **28,** 34.
13. Wiltshire, M. C. K. (1993) *GEC J. Res.* **10,** 119–125.
14. McOwan, P. W., Gordon, M. S. & Hossack, W. J. (1993) *Opt. Commun.* **103,** 189–193.
15. Ren, H., Fan, Y.-H. & Wu, S.-T. (2003) *Appl. Phys. Lett.* **83,** 1515–1517.
16. Laude, V. (1998) *Opt. Comm.* **153,** 134–152.
17. Hain, M., Glöckner, R., Bhattacharya, S., Dias, D., Stankovic, S. & Tschudi, T. (2001) *Opt. Comm.* **188,** 291–299.
18. Kress, B. & Mey, P. (2000) *Digital Diffractive Optics* (Wiley, New York).
19. Farn, M. W. & Veldkamp, W. B. (1994) in *Handbook of Optics*, ed. Bass, M. (McGraw–Hill, New York), Vol. II, Chap. 8, p. 8.15.
20. Brinkley, P. F., Kowel, S. T. & Chu, C. (1988) *Appl. Opt.* **27,** 4578–4586.
21. Apter, B., Efron, U. & Bahat-Treidel, E. (2004) *Appl. Opt.* **43,** 11–19.
22. Faklis, D. & Morris, G. M. (1995) *Appl. Opt.* **34,** 2462–2468.
23. Wu, S. T., Efron, U. & Hess, L. D. (1984) *Appl. Opt.* **23,** 3911–3915.
24. Williby, G. (2003) Ph.D. dissertation (Optical Sciences Center, Univ. of Arizona, Tucson, AZ).
25. INTELLIWAVE (1997) (Engineering Synthesis Design, Inc., Tucson, AZ).
26. Born, M. & Wolf, E. (1999) *Principles of Optics* (Cambridge Univ. Press, Cambridge, U.K.), 7th Ed.
27. Sales, T. R. M. & Morris, G. M. (1997) *Appl. Opt.* **36,** 253–257.
28. Wyant, J. C. & Creath, K. (1992) in *Applied Optics and Optical Engineering*, eds. Shannon, R. R. & Wyant, J. C. (Academic, London), Vol. XI, Chap. 1, p. 31.